HHS Public Access

Author manuscript

ACS Chem Biol. Author manuscript; available in PMC 2017 July 20.

Published in final edited form as:

ACS Chem Biol. 2016 June 17; 11(6): 1595–1602. doi:10.1021/acschembio.6b00043.

Structure of the Human Protein Kinase ZAK in Complex with Vemurafenib

Sebastian Mathea[1,2], **Kamal R. Abdul Azeez**[1], **Eidarus Salah**[1,2], **Cynthia Tallant**[1,2], **Finn Wolfreys**[2], **Rebecca Konietzny**[2], **Roman Fischer**[2], **Hua Jane Lou**[3], **Paul E. Brennan**[2], **Gisela Schnapp**[4], **Alexander Pautsch**[4], **Benedikt M. Kessler**[2], **Benjamin E. Turk**[3], and **Stefan Knapp**[2,5]

[1]Structural Genomics Consortium (SGC), Nuffield Department of Medicine, University of Oxford, Oxford, OX37DQ, UK

[2]Target Discovery Institute (TDI), Nuffield Department of Medicine, University of Oxford, Oxford, OX37FZ, UK

[3]Department of Pharmacology, Yale University School of Medicine, New Haven, CT 06520, USA

[4]Lead Discovery and Optimisation Support, Boehringer Ingelheim Pharma GmbH & Co KG, Biberach, 88400, Germany

[5]Institute for Pharmaceutical Chemistry and Buchmann Institute for Molecular Life Sciences (BMLS), Johann Wolfgang Goethe University, Frankfurt am Main, 60438, Germany

Abstract

The mixed lineage kinase ZAK is a key regulator of the MAPK pathway mediating cell survival and inflammatory response. ZAK is targeted by several clinically approved kinase inhibitors, and inhibition of ZAK has been reported to protect from doxorubicin-induced cardiomyopathy. On the other hand, unintended targeting of ZAK has been linked to severe adverse effects such as the development of cutaneous squamous cell carcinoma. Therefore, both specific inhibitors of ZAK, as well as anticancer drugs lacking off-target activity against ZAK, may provide therapeutic benefit. Here we report the first crystal structure of ZAK in complex with the B-RAF inhibitor vemurafenib. The co-crystal structure displayed a number of ZAK-specific features including a highly distorted P loop conformation enabling rational inhibitor design. Positional scanning peptide library analysis revealed a unique substrate specificity of the ZAK kinase including unprecedented preferences for histidine residues at positions −1 and +2 relative to the phosphoacceptor site. In addition, we screened a library of clinical kinase inhibitors identifying several inhibitors that potently inhibit ZAK, demonstrating that this kinase is commonly mistargeted by currently used anticancer drugs.

INTRODUCTION

The human leucine zipper- and sterile alpha motif-containing kinase (ZAK, also referred to as MLT, MLTK, HCCS-4, MRK and AZK) belongs to the mixed lineage kinase (MLK) family of protein kinases.(1) Its kinase domain shares about 40% sequence identity with other MLK family members such as MLK1 or DLK. Differential splicing leads to the expression of two ZAK isoforms.(2),(3) Besides the kinase domain, α-ZAK comprises a

leucine zipper, a SAM domain and a C terminal portion of unknown function. In the much shorter isoform β-ZAK, this C terminal portion including the SAM domain is replaced by a most likely disordered tail (Figure 1A). The comparison of cancer tissue with the adjacent normal tissue by transcriptome sequencing revealed that the ZAK isoforms were differentially expressed in colorectal, bladder and breast cancers with α-ZAK being higher expressed in the cancer tissue.(2),(4) However, whether the changes in isoform usage are causative for or a result of cell transformation is not clear yet.

Physiologically, ZAK has been classified as a MAP3K.(5) Its activation is induced by ribosomal stress(6), osmotic shock(7) and ionizing radiation(8), with PKN1 being a molecular trigger of ZAK activation(9), resulting in *trans*-autophosphorylation of ZAK activation loop residues T161 and S165(8). Once activated, ZAK phosphorylates MAP2K7 thus leading to JNK activation.(5) Since the JNK proteins regulate cellular processes such as apoptosis and inflammation(10) ZAK can be regarded as a key switch determining cell fate.

This property may be exploited for the development of cardioprotective drugs. ZAK is highly expressed in adult human cardiomyocytes(11),(12) and has been associated with cardiomyocyte hypertrophy(13). In a recent study, increased cellular ZAK activity led to enlarged cardiomyocytes and increased expression of the hypertrophy marker brain natriuretic peptide (BNP).(14) In support of a crucial role in cardiomyocyte signalling ZAK has been shown to be required for the activation of the MAPKs JNK and p38 by doxorubicin(15), a pathway that has been linked to the significant cardiotoxic adverse effects of this commonly used cytostatic agent(16),(17). A range of clinically used anticancer drugs that potently inhibit ZAK effectively suppressed doxorubicin-mediated phosphorylation of JNK and p38 thus potentially protecting the heart from doxorubicin-induced heart failure.(15) These drugs including nilotinib(18), ponatinib(15) and sorafenib(19) also resulted in down-regulation of inflammatory cytokines such as IL-1β and IL-6 suggesting anti-inflammatory properties of ZAK inhibition(15). The findings have been confirmed in ZAK-deficient mice, with doxorubicin failing to induce elevated serum levels of inflammatory cytokines.(15)

However, the role of ZAK as a regulator of apoptosis and cell survival has also been associated with common adverse effects of drugs with strong ZAK off-target activity(20),(21). The administration of these drugs induces the formation of cutaneous squamous cell carcinoma (cSCC), as reported for sorafenib (in 5–10% of all patients)(22), dabrafenib (6–11%)(23) and vemurafenib (20–26%)(24). Since many of the cSCC occur on sun-exposed skin areas, UV light has been assumed to be the trigger of cSCC development.(20) Both the knockdown of ZAK and the administration of compounds with ZAK inhibitory activity prevented UV light from inducing apoptosis in cancer cells.(20),(21) Moreover, ZAK inhibition accelerated the UV light-driven development of cSCC in the hairless mouse model.(20),(21) A prominent alternative model to explain cSCC formation is the inhibitor-driven paradoxical B-RAF activation.(25) Which model may be more valid under physiological conditions or whether both mechanisms cooperate to promote cSCC formation is still under debate.(26)

In order to provide a structural model for the development of ZAK-specific tool compounds and the design of kinase inhibitors that seek to avoid ZAK as an off-target, we report here the first high resolution structure of the ZAK kinase including the leucine zipper domain in complex with the B-RAF inhibitor vemurafenib. The unique binding mode of the inhibitor vemurafenib provides a structural model for the design of B-RAF inhibitors with improved specificity.

METHODS

Cloning, protein expression and purification

cDNA coding for ZAK residues 5 to 309 (Mammalian Gene Collection, MGC) was PCR amplified using the forward primer `TACTTCCAATCCATGGGTGCCTCCTTTGTGCA` and the reverse primer `TATCCACCTTTACTGTCATTTAAGCTCCTGCTCCTTAAAGC`. The PCR product was then inserted into the vector pFB-LIC-Bse via ligation independent cloning.(27) After the transposition of the coding sequence into an engineered Baculovirus genome (Bac-to-Bac, Invitrogen), the viral DNA was transfected into TriEx cells (Novagen) cultivated in InsectXpress medium (Lonza). Protein expression was performed as previously described.(28)

Cells were resuspended in lysis buffer (50 mM HEPES pH 7.4, 500 mM NaCl, 20 mM imidazole, 0.5 mM TCEP, 5% glycerol) and lysed by sonication. The lysate was cleared by centrifugation and loaded onto a Ni NTA column. After vigorous rinsing with lysis buffer the His_6 tagged protein was eluted in lysis buffer containing 300 mM imidazole. While the protein was subjected to dialysis to get rid of the imidazole the N terminal tag was cleaved by TEV protease. Contaminating proteins, the cleaved tag and TEV protease were removed by another Ni NTA step. Finally, $ZAK_{5–309}$ was concentrated and subjected to gel filtration using an AKTA Xpress system combined with an S200 gel filtration column. The elution volume 92.0 mL indicated the protein to be monomeric in solution. The final yield was 2.8 mg $ZAK_{5–309}$/1 L insect cell medium.

Crystallisation

50 nL of a solution containing 24 mg/mL $ZAK_{5–309}$ and 500 μM vemurafenib (20 mM HEPES pH 7.4, 150 mM NaCl, 0.5 mM TCEP, 5% glycerol) were transferred to a 3 well crystallisation plate (Swissci), mixed with 100 nL precipitant solution (100 mM bis-tris-propane pH 6.5, 200 mM sodium malonate, 20% PEG3350, 10% ethylene glycol) and incubated at 4°C. The slowly growing crystal was detected after 14 days and mounted after 42 days in precipitant solution cryoprotected with additional 20% ethylene glycol. Data were collected at Diamond Light Source, analysed, scaled and merged with Xia2(29). The structure was solved by molecular replacement with Phaser(30) using a MLK1 model as a template (PDB ID 3DTC) and refined with Refmac5(31). The model was validated using MolProbity(32). A summary of data collection and refinement statistics is given in Table S3. The model and the structure factors have been deposited with the PDB ID 5HES.

T_M shift assay

The assay was performed according to a previously established protocol.(33) A solution of 2 μM $ZAK_{5–309}$ in assay buffer (20 mM HEPES pH 7.4, 150 mM NaCl, 0.5 mM TCEP, 5% glycerol) was mixed 1:1000 with SYPRO Orange (Sigma). The compounds to be tested were added to a final concentration of 10 μM. 20 μL of each sample were placed in a 96-well plate and heated from 25 to 96°C. Fluorescence was monitored using a Mx3005P real-time PCR instrument (Stratagene) with excitation and emission filters set to 465 and 590 nm, respectively. Data were analysed with the MxPro software.

Kinase activity assay

ZAKtide (ANHWH**T**VHLRA) was synthesised by Micheal Berne (Tufts Medical School). 20 μM peptide were phosphorylated by 4 nM $ZAK_{5–309}$ in the presence of inhibitors (assay buffer 20 mM HEPES pH 7.4, 150 mM NaCl, 0.5 mM TCEP, 5% glycerol, 100 μM ATP, 5 mM $MgCl_2$). The reaction mixtures were incubated at 37°C for 1 hour before being quenched by the addition of formic acid to a final concentration of 1% (v/v). Both the substrate and product peptides were monitored by RapidFire™ mass spectrometry. Samples were loaded onto a C4 solid phase extraction (SPE) cartridge. The cartridge was then washed to remove non-volatile buffer salts using deionised water containing 0.1% formic acid (solvent A) at a flow rate of 1.5 mL/min for 4.5 s. The sample was eluted with acetonitrile containing 15% deionised water and 0.1% formic acid (solvent B) at a flow rate of 1.25 ml/min for 4.5 s. The eluent was analysed on an Agilent 6530 Accurate-Mass quadrupole time-of-flight (Q-TOF) mass spectrometer operated in positive ionisation mode. Ion chromatograms were extracted for the +3 charge state of the substrate (MW 1340.69 Da) and product (MW 1420.65 Da) and integrated using the RapidFire™ Integrator software. The ratio of product area to product plus substrate area was used as the response, and the baseline signal from a sample inactivated with formic acid prior to addition of substrate was subtracted. The data were fit to the following equation using the nls function in the R programming language:

$$\text{normalised response} = d + (a-d)/(1+10^{(\log \text{ inhibitor concentration} - \log \text{IC50}) \times \text{HillSlope}}).$$

Mean pIC50 was obtained by taking the geometric mean of pIC50s determined from duplicate experiments.

Isothermal titration calorimetry

Measurements were performed at 37°C on a MicroCal VP-ITC (GE Healthcare). $ZAK_{5–309}$ was dialysed overnight into assay buffer (20 mM HEPES pH 7.4, 150 mM NaCl, 0.5 mM TCEP, 5% glycerol). The syringe was loaded with 120 μM $ZAK_{5–309}$, the cell was filled with 15 μM vemurafenib. Every 10 minutes 10 μL of the protein solution were injected into the cell for a total of 28 injections. The heat flow data were analysed with the MicroCal ORIGIN software package employing a single binding site model.

Proteomic sample preparation

The samples were prepared as previously described.(34) In brief, protein samples were reduced and alkylated in solution and subjected to chloroform/methanol precipitation. The precipitate was resuspended in 6 M urea in 100 mM Tris pH 7.4, digested with elastase at 37°C overnight and desalted using C18 Sep Pak column cartridges (Waters). After drying down *in vacuo s*amples were resuspended in buffer A (98% H_2O, 2% acetonitrile, 0.1% formic acid).

Tandem mass spectrometry and data analysis

Samples were analysed using a nano-liquid chromatography tandem mass spectrometry (LC-MS/MS) system consisting of a Dionex Ultimate 3000 UPLC coupled to a hybrid quadrupole orbitrap instrument (Q Exactive, Thermo). Samples were loaded at a flow rate of 20 μL/min onto a PepMAP pre-column (C18, 300 μm×5mm, 5 μm particle size, Thermo) for one minute and separated at a flow rate of 250 nl/min on an nEASY column (C18, 75 μm×500 mm, 2 μm particle size, Thermo) for 60 minutes using a gradient of 2%–35% acetonitrile (v/v) in 5% DMSO (v/v) and 0.1% formic acid (v/v). All scans were performed at a resolution of 70,000 at 200 mass/charge and the 15 most abundant precursors were selected for HCD fragmentation. Raw MS data were *de novo* sequenced by PEAKS Version 7 (Bioinformatics Solutions) with search criteria at 10 ppm for MS^1 and 0.05 Da for MS^2. A database search (human SwissProt, 85,809 sequences) with subsequent posttranslational modification searches, where all modifications reported in UNIMOD were considered, was then applied to the *de novo* identified MS/MS spectra. False discovery rates of 1% threshold were applied. MS/MS spectra with phosphorylation modifications were inspected manually.

Peptide library screening

The library consisted of 182 peptide mixtures and was arrayed in a 1536-well plate at 50 μM concentration in 2 μL reaction buffer (50 mM Tris, pH 7.5, 10 mM $MgCl_2$, 2 mM $MnCl_2$, 0.1 mM EGTA, 1 mM DTT, 0.1% Tween 20) per well. Peptide mixtures had the general sequence Y-A-X-X-X-X-X-S/T-X-X-X-X-A-G-K-K(biotin).(35) In each well in the array, one of the X positions was fixed as a single amino acid at the indicated position, while the others were an equimolar mixture of the 17 amino acids excluding cysteine, serine and threonine. Two additional peptide mixtures were included that fixed either Ser or Thr at the phosphoacceptor position with all X positions left as mixtures. Purified ZAK was added to 10 – 30 μg/μL concentration along with ATP (to 50 μM including 0.03 μCi/μL γ-[^{33}P]ATP), and plates were sealed and incubated at 30°C for 2 hours. Aliquots (200 nL) from each well were then spotted onto a streptavidin membrane (Promega), which was extensively washed, air-dried, and exposed to a phosphor screen to quantify radiolabel incorporation into each peptide. Quantified signals were normalized so that the average value of all amino acids at a given position were equal to 1. The heat map was generated in Microsoft Excel following $\log_2$ transformation of the normalized data.

RESULTS AND DISCUSSION

Inhibitor screen

Both α-ZAK and β-ZAK comprise the kinase domain and the leucine zipper (Figure 1A). This region of the protein was chosen for structural analysis. To aid crystallization trials, we tested a small kinase inhibitor library (~150 compounds that have been approved or have been in clinical trials before 2012, purchased from Selleckchem) using a melting temperature (T_M) shift assay(36). In this assay inhibitor binding is assessed by a shift in melting temperature of the target protein that usually linearly correlates with inhibitor binding strength.(37) In agreement with earlier reports nilotinib(18), sorafenib(19), dabrafenib(21) and vemurafenib(21),(38) significantly increased T_M for ZAK supporting strong interaction with the kinase (Figure 1B,E). With this simple assay we identified not only the inhibitors already reported to bind ZAK but also additional clinical inhibitors with significant activity for ZAK as judged by their T_M increase (Table S1). Ponatinib induced with 15°C the highest T_M shift. The phosphorylation of ZAK in the activation loop residues T161 and S165 had no impact on the stabilisation pattern. Interestingly, most of the identified ZAK stabilisers were type II inhibitors capable of binding kinases in the DFG-out conformation (type II inhibitors have been marked with an asterisk in Figure 1E).

ZAK kinase substrate specificity

ZAK is a catalytically active kinase.(8) Testing ZAK for its ability to phosphorylate a combinatorial peptide library(35) revealed a unique substrate specificity (Figure 1C and Table S2). Besides preferring threonine as the phosphoacceptor, ZAK was selective for hydrophobic residues at positions +1 (AVIFY) and +3 (VFYWQ) from the phosphoacceptor. The additional preferences (tryptophan at −2, histidines at −1 and +2) have not been previously reported for a kinase. While the sequence flanking the primary ZAK autophosphorylation site T161 (`RFHNH`**`T`**`THMS`) corresponded well to the determined consensus sequence (Figure 1C), the secondary ZAK autophosphorylation site S165 (`HTTHM`**`S`**`LVGT`) was a more distant match to the consensus sequence. Interestingly, even the activation segments of the physiological ZAK substrates MAP2K4 (`GQLVD`**`S`**`IAKT`) and MAP2K7 (`GRLVD`**`S`**`KAKT`) are predicted to be poor ZAK substrates as isolated peptides. These findings suggest that selective and efficient substrate targeting by ZAK involves complex formation with downstream signalling factors, which has been generally observed for MAP3K interactions with MAP2Ks(39).

Validation of T_M shift hits with a kinase activity assay

The optimal ZAK peptide substrate (ZAKtide, `ANHWH`**`T`**`VHLRA`) was synthesised (Michael Berne, Tufts Medical School) and served as the substrate in a kinase activity assay. ZAKtide was incubated with ZAK and ATP/Mg^{2+} at 37°C, and the relative levels of unphosphorylated and phosphorylated ZAKtide in the reaction mixture were quantified using mass spectrometry. Under the chosen conditions the apparent K_M value for ATP was determined to be 140 μM which is in the range of K_M values for previously investigated protein kinases(40). We measured IC50 values for compounds that stabilised ZAK by more than 5°C in T_M shift assay (Figures 1D and S1). All of the tested compounds inhibited ZAK

with IC50s ranging from 12 nM for rebastinib to 210 nM for apatinib confirming the T_M shift data (Figure 1E). However, probably due to differences in binding modes T_M shift values did not always correlate well with experimental IC50 values.

ZAK crystallisation

Our attempts to co-crystallise ZAK with ATP-γ-S and a subset of the T_M shift hits (ponatinib, motesanib and vemurafenib) were not successful (summarised in Figure 2B). Though ZAK crystallised in complex with ATP-γ-S the diffraction was poor. Therefore, ZAK was subjected to autophoshorylation resulting in ZAK that was monophosphorylated mainly at the activation loop residue T161 (Figures 2C,D and S2) and ZAK diphosphorylated at T161 and S165. These differentially phosphorylated ZAK variants were co-crystallised with the inhibitors mentioned above. Only the combination of monophosphorylated ZAK and vemurafenib resulted in crystals with suitable diffraction properties. The structure was solved by molecular replacement using a MLK1 model (PDB ID 3DTC) as a template. A summary of data collection and refinement statistics is given in Table S3.

Structure of the ZAK-vemurafenib complex

The ZAK kinase domain comprised the canonical kinase catalytic domain structure with an N lobe containing the β1-β5 sheets and the αC helix and the mainly helical C lobe. As expected, the inhibitor vemurafenib interacted with the ATP binding site (Figure 2A). Besides this conserved architecture common to all protein kinases the ZAK structure revealed some unique features.

The αC helix is predicted by PSIPRED to comprise residues 48–59. However, in the crystal structure it was moved away from the ATP binding site and comprised only residues 53–59. This SRC/CDK-like inactive conformation was probably due to the interaction with vemurafenib which pushed the αC helix outward. As a result the conserved salt bridge between K45 and E53 which is regarded a hallmark for the active kinase conformation was not formed (Figure S3).

The ZAK kinase and SAM domains are linked by 60 residues that are predicted to comprise a leucine zipper. The helix in the N terminus of the linker was attached to the kinase C lobe. W283 formed a π stacking interaction with F276, while L291, L294 and L297 formed a hydrophobic surface patch interacting with residues located in the αG helix (Figure 2F). The C terminus of the linker was not resolved in the structure with the electron density dropping sharply after residue 299. Based on the prediction of helical secondary structure for residues 301–322 we assume that the linker is composed of two helices interconnected by a flexible hinge. For Nek2, another protein kinase with a leucine zipper succeeding the kinase domain, the leucine zipper is required for homodimerisation and activation.(41) It remains to be investigated if a similar mechanism is also valid for ZAK. However, our construct $ZAK_{5–309}$ did neither dimerise in size exclusion chromatography nor did the leucine zippers interact in the crystal.

The conserved P loop typically constitutes the most flexible part of the kinase N lobe. It bridges the β1 and β2 sheets and contributes to position the ATP β- and γ-phosphates for

catalysis. In kinases bound to ATP and in 98% of the publicly available structures of kinase-inhibitor complexes, the P loop adopts an extended conformation.(42) However, in the ZAK-vemurafenib complex, the P loop was folded over the inhibitor thus forming a hydrophobic cage. This kinked conformation was mainly driven by the G23 backbone amide having polar contacts with the vemurafenib chlorine atom and by F27 forming a π stacking interaction with the chlorophenyl moiety.

As mentioned above ZAK tightly bound to a range of type II kinase inhibitors suggesting that the ZAK DFG motif at the base of the activation loop is capable of adopting the DFG-out conformation. However, the bound vemurafenib stabilised the DFG-in conformation with D151 pointing towards the ATP binding pocket and F152 pointing towards the αC β4 loop that anchors the C terminus of the αC helix to the top of the C lobe (Figure 2E). The protein used for crystallisation was phosphorylated in the activation loop residue T161 (Figures 2C,D and S2). In the crystal structure, the phosphate moiety of pT161 was in proximity of E51 N terminal of the αC helix, H158 in the activation loop and C285 of a neighbouring ZAK molecule interacting through crystal contacts. This interaction seems to be indispensable for crystallisation in space group P 4_1 since we did not obtain any such crystals of ZAK in a different phosphorylation state. The location of pT161 in the crystal structure is surprising as this phosphorylation site is located at the expected position in the sequence for activating phosphorylation sites (approximately 11 residues N terminal of the APE helix) and is expected to anchor the activation segment to the HRD arginine. It remains therefore to be investigated if the observed conformation is a consequence of inhibitor binding or may also be observed in the apoprotein. The region C terminal of pT161 was not resolved in the experimental electron density creating a 6 residue gap and indicating a disordered activation loop in solution despite its phosphorylated state. We speculate that T161 phosphorylation alone may not be sufficient to induce the attachment of the activation loop to the C lobe indicating additional S165 phosphorylation to be required to achieve full ZAK activity.

Thermodynamics of vemurafenib binding to ZAK

In order to determine the thermodynamic parameters for the binding of vemurafenib to ZAK in solution we performed isothermal titration calorimetry (ITC). Due to the poor vemurafenib solubility the experimental setup had to be optimised. Finally we carried out the binding experiment as a reverse titration in which a solution of 120 μM unphosphorylated ZAK was titrated into 15 μM vemurafenib at 37°C (Figure 3A). The binding was enthalpically driven ($\Delta H = -9.6$ kcal·mol^{-1}) with a minor entropic contribution to binding ($-T\Delta S = -1.1$ kcal·mol^{-1}) resulting in a dissociation constant (K_D) of 29 ± 4 nM. The slow equilibration following the injections likely reflected structural rearrangements within ZAK. Takeninto account the tight binding of type II inhibitors we suggest that in solution both the ZAK DFG-in and DFG-out conformations prevail in equilibrium, and that the interconversion rates are low. The measured K_D was consistent with the measured IC50 value of 23 ± 4 nM (Figure 1D) and with KINOMEscan data of the close vemurafenib analogue PLX4720 to ZAK with a K_D of 41 nM.(38) The insertion of the phenyl ring into PLX4720 was reported to increase the inhibitor's affinity for ZAK by factor 2.(21)

Vemurafenib binding mode

Our structural model suggests that vemurafenib does not inhibit ZAK by simply blocking the ATP binding site but by significantly distorting the kinase fold. Vemurafenib tightly interacted with five ZAK structural motifs (Figure 3B). The central 7-azaindole firmly anchored vemurafenib in the position generally occupied by the ATP purine forming two ATP mimetic hydrogen bonds with the backbone of E83 and A85 in the ZAK hinge region. The interaction was further strengthened by a π stacking interaction of Y84 with the condensed ring system.

The bifluorinated phenyl ring substituted with a propylsulfonamide group interacted with the DFG motif and penetrated with the propyl moiety into a pocket formed by the displaced αC helix and the DFG motif. Three hydrogen bonds were formed with all backbone nitrogens of the DFG motif thus trapping it in the DFG-in conformation. A water bridge interconnected the vemurafenib ketone linker and the D151 side chain contributing additional interactions with ZAK.

The second substituent of the 7-azaindole in vemurafenib is a chlorophenyl ring in 5 position. Even though the ring protruded from the ATP binding site it was entwined by the displaced ZAK P loop thus shielded from the surrounding solvent. The main driving force of the kinked P loop conformation seemed to be a π stacking interaction of F27 with the chlorophenyl ring.

Comparison of B-RAF and ZAK bound to vemurafenib

The vemurafenib binding modes in B-RAF and ZAK share the same hinge interaction, but they differ considerably in the P loop conformation. While in B-RAF the P loop adopts an extended conformation not making contacts to vemurafenib(43), the ZAK P loop extensively interacts with vemurafenib (Figure 3D,E). The inhibitor PLX4720 differs from vemurafenib by the substitution of the chlorophenyl ring for a chlorine atom (Figure 3C).(43) The affinities of PLX4720 and vemurafenib for ZAK and B-RAF have been determined by a KINOMEscan competitive binding assay.(21) PLX4720 is a more potent inhibitor for B-RAF when compared with vemurafenib (IC50s 32 nM vs 65 nM), for ZAK this property is reversed (IC50s 9.5 nM vs 4.0 nM).(21) Our structural data suggest that this is due to the P loop interacting with the chlorophenyl ring. Folded and distorted P loop conformations have been associated with favourable inhibitor selectivity.(42) A structural consequence of a folded P loop, in particular when it is associated with an αC out movement, is the generation of a cavity between the P loop and αC. Such a cavity has for instance successfully targeted by the ERK inhibitor SCH772984.(44) The structure of the vemurafenib ZAK complex revealed a similar binding pocket extending from the carbonyl moiety of the inhibitor suggesting that this structural feature could be explored for the generation of selective ZAK inhibitors. Distortion of the P loop has also been linked to the specificity of imatinib for the tyrosine kinase ABL over c-SRC. The K_D for imatinib binding ABL is by factor 2300 lower than for c-SRC(45) despite the high conservation of both binding sites. Besides the more favoured DFG-out conformation in ABL it is the P loop conformation (kinked in ABL(46) and extended in c-SRC(45)) that accounts for the difference.(47),(48),(49)

Impact on rational drug design

Vemurafenib has low nanomolar activity for a range of kinases, but its highest activity is displayed towards ZAK.(21) It is therefore likely that the vemurafenib scaffold can serve as a starting point for the development of more selective ZAK inhibitors. ZAK is the only human kinase bearing a cysteine residue in P loop −1 position.(50) In the ZAK/vemurafenib complex, this cysteine is in close proximity to the vemurafenib chlorophenyl moiety. Taken together, the replacement of the chlorophenyl moiety by an adequate electrophilic warhead could potentially lead to a specific covalent ZAK inhibitor. This strategy has been successfully employed for a number of kinases such as JAK3(51) and CDK7(52).

Likewise, the insights into the binding mode of vemurafenib to ZAK might help to generate inhibitors with increased B-RAF selectivity. For pharmacological reasons vemurafenib, and not PLX4720, was chosen to be tested in clinical trials(43), even though the introduction of the chlorophenyl moiety decreased the affinity of the inhibitor for B-RAF(21). It was previously not known that the improved pharmacological profile had to be paid by increased off-target activity towards ZAK. The chlorophenyl moiety interacts with ZAK F27 and D92. Replacing the chlorophenyl moiety by a substituent that retains the pharmacological profile but prevents the interaction with ZAK F27 and D92 might lead to a drug with reduced adverse effects.

CONCLUSIONS

Here we provided the first structural model for the common off-target of clinically approved kinase inhibitors ZAK. Inhibition of this kinase has been linked to significant adverse effects of currently used drugs, and the structural insight provided by the ZAK complex with the B-RAF inhibitor vemurafenib suggests new rational design strategies avoiding unintended ZAK inhibition by future drug candidates. The excellent druggability of ZAK demonstrated by our limited inhibitor screening campaign using a clinical kinase inhibitor set together with the presented unique structural features may also lead to highly selective ZAK inhibitors that may find applications as cardioprotective agents during chemotherapy or as new inhibitors treating heart failure and fibrosis as well as inflammatory conditions.

Supplementary Material

Refer to Web version on PubMed Central for supplementary material.

Acknowledgments

SM is grateful for support by Boehringer Ingelheim. The SGC is a registered charity (number 1097737) that receives funds from AbbVie, Bayer, Boehringer Ingelheim, the Canada Foundation for Innovation, the Canadian Institutes for Health Research, Genome Canada, GlaxoSmithKline, Janssen, Lilly Canada, the Novartis Research Foundation, the Ontario Ministry of Economic Development and Innovation, Pfizer, Takeda, and the Wellcome Trust [092809/Z/10/Z]. BMK is supported by the John Fell Fund 133/075 and the Wellcome Trust [097813/Z/11/Z].

References

1. Manning G, Whyte DB, Martinez R, Hunter T, Sudarsanam S. The protein kinase complement of the human genome. Science. 2002; 298:1912–1934. [PubMed: 12471243]

2. Liu J, McCleland M, Stawiski EW, Gnad F, Mayba O, Haverty PM, Durinck S, Chen YJ, Klijn C, Jhunjhunwala S, Lawrence M, Liu H, Wan Y, Chopra V, Yaylaoglu MB, Yuan W, Ha C, Gilbert HN, Reeder J, Pau G, Stinson J, Stern HM, Manning G, Wu TD, Neve RM, de Sauvage FJ, Modrusan Z, Seshagiri S, Firestein R, Zhang Z. Integrated exome and transcriptome sequencing reveals ZAK isoform usage in gastric cancer. Nat Commun. 2014; 5:3830. [PubMed: 24807215]

3. Bloem LJ, Pickard TR, Acton S, Donoghue M, Beavis RC, Knierman MD, Wang X. Tissue distribution and functional expression of a cDNA encoding a novel mixed lineage kinase. J Mol Cell Cardiol. 2001; 33:1739–1750. [PubMed: 11549352]

4. Rey C, Faustin B, Mahouche I, Ruggieri R, Brulard C, Ichas F, Soubeyran I, Lartigue L, De Giorgi F. The MAP3K ZAK, a novel modulator of ERK-dependent migration, is upregulated in colorectal cancer. Oncogene. 2015

5. Yang JJ. Mixed lineage kinase ZAK utilizing MKK7 and not MKK4 to activate the c-Jun N-terminal kinase and playing a role in the cell arrest. Biochem Biophys Res Commun. 2002; 297:105–110. [PubMed: 12220515]

6. Jandhyala DM, Ahluwalia A, Obrig T, Thorpe CM. ZAK: a MAP3Kinase that transduces Shiga toxin- and ricin-induced proinflammatory cytokine expression. Cell Microbiol. 2008; 10:1468–1477. [PubMed: 18331592]

7. Mao X, Bravo IG, Cheng H, Alonso A. Multiple independent kinase cascades are targeted by hyperosmotic stress but only one activates stress kinase p38. Exp Cell Res. 2004; 292:304–311. [PubMed: 14697338]

8. Tosti E, Waldbaum L, Warshaw G, Gross EA, Ruggieri R. The stress kinase MRK contributes to regulation of DNA damage checkpoints through a p38gamma-independent pathway. J Biol Chem. 2004; 279:47652–47660. [PubMed: 15342622]

9. Takahashi M, Gotoh Y, Isagawa T, Nishimura T, Goyama E, Kim HS, Mukai H, Ono Y. Regulation of a mitogen-activated protein kinase kinase kinase, MLTK by PKN. J Biochem. 2003; 133:181–187. [PubMed: 12761180]

10. Davies C, Tournier C. Exploring the function of the JNK (c-Jun N-terminal kinase) signalling pathway in physiological and pathological processes to design novel therapeutic strategies. Biochem Soc Trans. 2012; 40:85–89. [PubMed: 22260670]

11. Liu TC, Huang CJ, Chu YC, Wei CC, Chou CC, Chou MY, Chou CK, Yang JJ. Cloning and expression of ZAK, a mixed lineage kinase-like protein containing a leucine-zipper and a sterile-alpha motif. Biochem Biophys Res Commun. 2000; 274:811–816. [PubMed: 10924358]

12. Fuller SJ, Osborne SA, Leonard SJ, Hardyman MA, Vaniotis G, Allen BG, Sugden PH, Clerk A. Cardiac protein kinases: the cardiomyocyte kinome and differential kinase expression in human failing hearts. Cardiovasc Res. 2015; 108:87–98. [PubMed: 26260799]

13. Huang CY, Kuo WW, Chueh PJ, Tseng CT, Chou MY, Yang JJ. Transforming growth factor-beta induces the expression of ANF and hypertrophic growth in cultured cardiomyoblast cells through ZAK. Biochem Biophys Res Commun. 2004; 324:424–431. [PubMed: 15465036]

14. Hsieh YL, Tsai YL, Shibu MA, Su CC, Chung LC, Pai P, Kuo CH, Yeh YL, Viswanadha VP, Huang CY. ZAK induces cardiomyocyte hypertrophy and brain natriuretic peptide expression via p38/JNK signaling and GATA4/c-Jun transcriptional factor activation. Mol Cell Biochem. 2015; 405:1–9. [PubMed: 25869677]

15. Wong J, Smith LB, Magun EA, Engstrom T, Kelley-Howard K, Jandhyala DM, Thorpe CM, Magun BE, Wood LJ. Small molecule kinase inhibitors block the ZAK-dependent inflammatory effects of doxorubicin. Cancer Biol Ther. 2013; 14:56–63. [PubMed: 23114643]

16. Lefrak EA, Pitha J, Rosenheim S, Gottlieb JA. A clinicopathologic analysis of adriamycin cardiotoxicity. Cancer. 1973; 32:302–314. [PubMed: 4353012]

17. Nobori K, Ito H, Tamamori-Adachi M, Adachi S, Ono Y, Kawauchi J, Kitajima S, Marumo F, Isobe M. ATF3 inhibits doxorubicin-induced apoptosis in cardiac myocytes: a novel cardioprotective role of ATF3. J Mol Cell Cardiol. 2002; 34:1387–1397. [PubMed: 12392999]

18. Manley PW, Drueckes P, Fendrich G, Furet P, Liebetanz J, Martiny-Baron G, Mestan J, Trappe J, Wartmann M, Fabbro D. Extended kinase profile and properties of the protein kinase inhibitor nilotinib. Biochim Biophys Acta. 2010; 1804:445–453. [PubMed: 19922818]

19. Karaman MW, Herrgard S, Treiber DK, Gallant P, Atteridge CE, Campbell BT, Chan KW, Ciceri P, Davis MI, Edeen PT, Faraoni R, Floyd M, Hunt JP, Lockhart DJ, Milanov ZV, Morrison MJ, Pallares G, Patel HK, Pritchard S, Wodicka LM, Zarrinkar PP. A quantitative analysis of kinase inhibitor selectivity. Nat Biotechnol. 2008; 26:127–132. [PubMed: 18183025]
20. Vin H, Ching G, Ojeda SS, Adelmann CH, Chitsazzadeh V, Dwyer DW, Ma H, Ehrenreiter K, Baccarini M, Ruggieri R, Curry JL, Ciurea AM, Duvic M, Busaidy NL, Tannir NM, Tsai KY. Sorafenib suppresses JNK-dependent apoptosis through inhibition of ZAK. Mol Cancer Ther. 2014; 13:221–229. [PubMed: 24170769]
21. Vin H, Ojeda SS, Ching G, Leung ML, Chitsazzadeh V, Dwyer DW, Adelmann CH, Restrepo M, Richards KN, Stewart LR, Du L, Ferguson SB, Chakravarti D, Ehrenreiter K, Baccarini M, Ruggieri R, Curry JL, Kim KB, Ciurea AM, Duvic M, Prieto VG, Ullrich SE, Dalby KN, Flores ER, Tsai KY. BRAF inhibitors suppress apoptosis through off-target inhibition of JNK signaling. Elife. 2013; 2:e00969. [PubMed: 24192036]
22. Dubauskas Z, Kunishige J, Prieto VG, Jonasch E, Hwu P, Tannir NM. Cutaneous squamous cell carcinoma and inflammation of actinic keratoses associated with sorafenib. Clin Genitourin Cancer. 2009; 7:20–23. [PubMed: 19213663]
23. Hauschild A, Grob JJ, Demidov LV, Jouary T, Gutzmer R, Millward M, Rutkowski P, Blank CU, Miller WH Jr, Kaempgen E, Martin-Algarra S, Karaszewska B, Mauch C, Chiarion-Sileni V, Martin AM, Swann S, Haney P, Mirakhur B, Guckert ME, Goodman V, Chapman PB. Dabrafenib in BRAF-mutated metastatic melanoma: a multicentre, openlabel, phase 3 randomised controlled trial. Lancet. 2012; 380:358–365. [PubMed: 22735384]
24. Chapman PB, Hauschild A, Robert C, Haanen JB, Ascierto P, Larkin J, Dummer R, Garbe C, Testori A, Maio M, Hogg D, Lorigan P, Lebbe C, Jouary T, Schadendorf D, Ribas A, O'Day SJ, Sosman JA, Kirkwood JM, Eggermont AM, Dreno B, Nolop K, Li J, Nelson B, Hou J, Lee RJ, Flaherty KT, McArthur GA. Improved survival with vemurafenib in melanoma with BRAF V600E mutation. N Engl J Med. 2011; 364:2507–2516. [PubMed: 21639808]
25. Hatzivassiliou G, Song K, Yen I, Brandhuber BJ, Anderson DJ, Alvarado R, Ludlam MJ, Stokoe D, Gloor SL, Vigers G, Morales T, Aliagas I, Liu B, Sideris S, Hoeflich KP, Jaiswal BS, Seshagiri S, Koeppen H, Belvin M, Friedman LS, Malek S. RAF inhibitors prime wild-type RAF to activate the MAPK pathway and enhance growth. Nature. 2010; 464:431–435. [PubMed: 20130576]
26. Holderfield M, Nagel TE, Stuart DD. Mechanism and consequences of RAF kinase activation by small-molecule inhibitors. Br J Cancer. 2014; 111:640–645. [PubMed: 24642617]
27. Strain-Damerell C, Mahajan P, Gileadi O, Burgess-Brown NA. Medium-throughput production of recombinant human proteins: ligation-independent cloning. Methods Mol Biol. 2014; 1091:55–72. [PubMed: 24203324]
28. Mahajan P, Strain-Damerell C, Gileadi O, Burgess-Brown NA. Medium-throughput production of recombinant human proteins: protein production in insect cells. Methods Mol Biol. 2014; 1091:95–121. [PubMed: 24203326]
29. Winter G. xia2: an expert system for macromolecular crystallography data reduction. Journal of Applied Crystallography. 2010; 43:186–190.
30. McCoy AJ, Grosse-Kunstleve RW, Storoni LC, Read RJ. Likelihood-enhanced fast translation functions. Acta Crystallogr D Biol Crystallogr. 2005; 61:458–464. [PubMed: 15805601]
31. Murshudov GN, Vagin AA, Dodson EJ. Refinement of macromolecular structures by the maximum-likelihood method. Acta Crystallogr D Biol Crystallogr. 1997; 53:240–255. [PubMed: 15299926]
32. Chen VB, Arendall WB 3rd, Headd JJ, Keedy DA, Immormino RM, Kapral GJ, Murray LW, Richardson JS, Richardson DC. MolProbity: all-atom structure validation for macromolecular crystallography. Acta Crystallogr D Biol Crystallogr. 2010; 66:12–21. [PubMed: 20057044]
33. Niesen FH, Berglund H, Vedadi M. The use of differential scanning fluorimetry to detect ligand interactions that promote protein stability. Nat Protoc. 2007; 2:2212–2221. [PubMed: 17853878]
34. Wijnhoven P, Konietzny R, Blackford AN, Travers J, Kessler BM, Nishi R, Jackson SP. USP4 Auto-Deubiquitylation Promotes Homologous Recombination. Mol Cell. 2015; 60:362–373. [PubMed: 26455393]

35. Miller CJ, Turk BE. Rapid Identification of Protein Kinase Phosphorylation Site Motifs Using Combinatorial Peptide Libraries. Methods Mol Biol. 2016; 1360:203–216. [PubMed: 26501912]
36. Fedorov O, Niesen FH, Knapp S. Kinase inhibitor selectivity profiling using differential scanning fluorimetry. Methods Mol Biol. 2012; 795:109–118. [PubMed: 21960218]
37. Fedorov O, Huber K, Eisenreich A, Filippakopoulos P, King O, Bullock AN, Szklarczyk D, Jensen LJ, Fabbro D, Trappe J, Rauch U, Bracher F, Knapp S. Specific CLK inhibitors from a novel chemotype for regulation of alternative splicing. Chem Biol. 2011; 18:67–76. [PubMed: 21276940]
38. Davis MI, Hunt JP, Herrgard S, Ciceri P, Wodicka LM, Pallares G, Hocker M, Treiber DK, Zarrinkar PP. Comprehensive analysis of kinase inhibitor selectivity. Nat Biotechnol. 2011; 29:1046–1051. [PubMed: 22037378]
39. Takekawa M, Tatebayashi K, Saito H. Conserved docking site is essential for activation of mammalian MAP kinase kinases by specific MAP kinase kinase kinases. Mol Cell. 2005; 18:295–306. [PubMed: 15866172]
40. Knight ZA, Shokat KM. Features of selective kinase inhibitors. Chem Biol. 2005; 12:621–637. [PubMed: 15975507]
41. Fry AM, Arnaud L, Nigg EA. Activity of the human centrosomal kinase, Nek2, depends on an unusual leucine zipper dimerization motif. J Biol Chem. 1999; 274:16304–16310. [PubMed: 10347187]
42. Guimaraes CR, Rai BK, Munchhof MJ, Liu S, Wang J, Bhattacharya SK, Buckbinder L. Understanding the impact of the P-loop conformation on kinase selectivity. J Chem Inf Model. 2011; 51:1199–1204. [PubMed: 21568278]
43. Bollag G, Hirth P, Tsai J, Zhang J, Ibrahim PN, Cho H, Spevak W, Zhang C, Zhang Y, Habets G, Burton EA, Wong B, Tsang G, West BL, Powell B, Shellooe R, Marimuthu A, Nguyen H, Zhang KY, Artis DR, Schlessinger J, Su F, Higgins B, Iyer R, D'Andrea K, Koehler A, Stumm M, Lin PS, Lee RJ, Grippo J, Puzanov I, Kim KB, Ribas A, McArthur GA, Sosman JA, Chapman PB, Flaherty KT, Xu X, Nathanson KL, Nolop K. Clinical efficacy of a RAF inhibitor needs broad target blockade in BRAF-mutant melanoma. Nature. 2010; 467:596–599. [PubMed: 20823850]
44. Chaikuad A, Tacconi EM, Zimmer J, Liang Y, Gray NS, Tarsounas M, Knapp S. A unique inhibitor binding site in ERK1/2 is associated with slow binding kinetics. Nat Chem Biol. 2014; 10:853–860. [PubMed: 25195011]
45. Seeliger MA, Nagar B, Frank F, Cao X, Henderson MN, Kuriyan J. c-Src binds to the cancer drug imatinib with an inactive Abl/c-Kit conformation and a distributed thermodynamic penalty. Structure. 2007; 15:299–311. [PubMed: 17355866]
46. Nagar B, Hantschel O, Young MA, Scheffzek K, Veach D, Bornmann W, Clarkson B, Superti-Furga G, Kuriyan J. Structural basis for the autoinhibition of c-Abl tyrosine kinase. Cell. 2003; 112:859–871. [PubMed: 12654251]
47. Dar AC, Lopez MS, Shokat KM. Small molecule recognition of c-Src via the Imatinib-binding conformation. Chem Biol. 2008; 15:1015–1022. [PubMed: 18940662]
48. Seeliger MA, Ranjitkar P, Kasap C, Shan Y, Shaw DE, Shah NP, Kuriyan J, Maly DJ. Equally potent inhibition of c-Src and Abl by compounds that recognize inactive kinase conformations. Cancer Res. 2009; 69:2384–2392. [PubMed: 19276351]
49. Lin YL, Meng Y, Jiang W, Roux B. Explaining why Gleevec is a specific and potent inhibitor of Abl kinase. Proc Natl Acad Sci U S A. 2013; 110:1664–1669. [PubMed: 23319661]
50. Liu Q, Sabnis Y, Zhao Z, Zhang T, Buhrlage SJ, Jones LH, Gray NS. Developing irreversible inhibitors of the protein kinase cysteinome. Chem Biol. 2013; 20:146–159. [PubMed: 23438744]
51. Tan L, Akahane K, McNally R, Reyskens KM, Ficarro SB, Liu S, Herter-Sprie GS, Koyama S, Pattison MJ, Labella K, Johannessen L, Akbay EA, Wong KK, Frank DA, Marto JA, Look TA, Arthur JS, Eck MJ, Gray NS. Development of Selective Covalent Janus Kinase 3 Inhibitors. J Med Chem. 2015; 58:6589–6606. [PubMed: 26258521]
52. Kwiatkowski N, Zhang T, Rahl PB, Abraham BJ, Reddy J, Ficarro SB, Dastur A, Amzallag A, Ramaswamy S, Tesar B, Jenkins CE, Hannett NM, McMillin D, Sanda T, Sim T, Kim ND, Look T, Mitsiades CS, Weng AP, Brown JR, Benes CH, Marto JA, Young RA, Gray NS. Targeting

transcription regulation in cancer with a covalent CDK7 inhibitor. Nature. 2014; 511:616–620. [PubMed: 25043025]

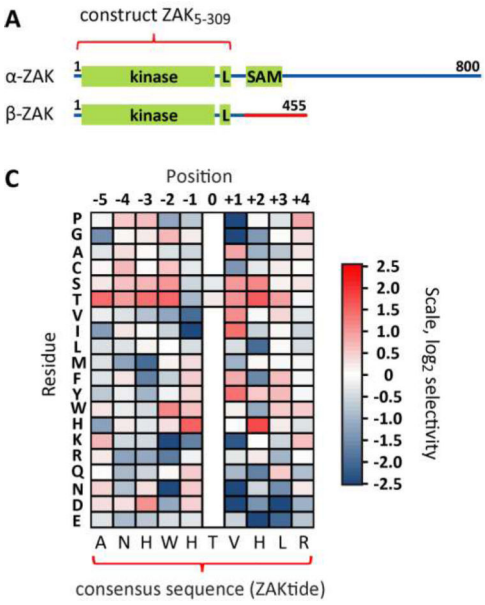

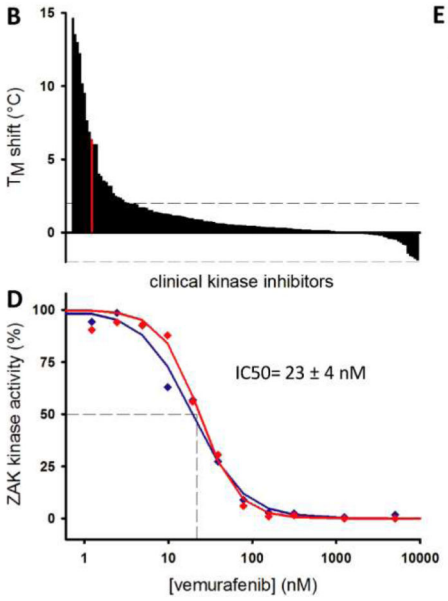

E

Inhibitor	T_M shift (°C)	IC50 (nM)
Ponatinib*	15	42 ± 4
Rebastinib*	14	12 ± 2
Regorafenib*	13	28 ± 3
Sorafenib*	12	22 ± 2
Motesanib*	10	130 ± 10
RAF265*	9.6	12 ± 3
Dabrafenib	7.7	22 ± 10
Bafetinib*	6.9	38 ± 16
Vemurafenib	6.4	23 ± 4
Apatinib*	6.1	210 ± 30
Nilotinib*	6.1	42 ± 5

Figure 1.

(A) Domain architecture of ZAK splicing isoforms. The construct $ZAK_{5–309}$ comprises the region of the protein shared by both isoforms. **(B)** Clinical kinase inhibitors bind and stabilise $ZAK_{5–309}$ as judged by T_M shift assay. A list of T_M shifts is given in Table S1. **(C)** ZAK linear substrate specificity determined by screening combinatorial peptide libraries. The heat map shows the average normalised signals from three replicates. Quantified data are given in Table S2. The derived consensus peptide (ZAKtide) is shown below the heat map. **(D)** Vemurafenib inhibits ZAK kinase activity with an IC50 of 23 nM. The experiment was performed in duplicate and both datasets are shown. **(E)** The clinical kinase inhibitors with the highest activity for ZAK in T_M shift assay. Binding was validated by the inhibition of ZAK kinase activity. Type II inhibitors are marked with an asterisk.

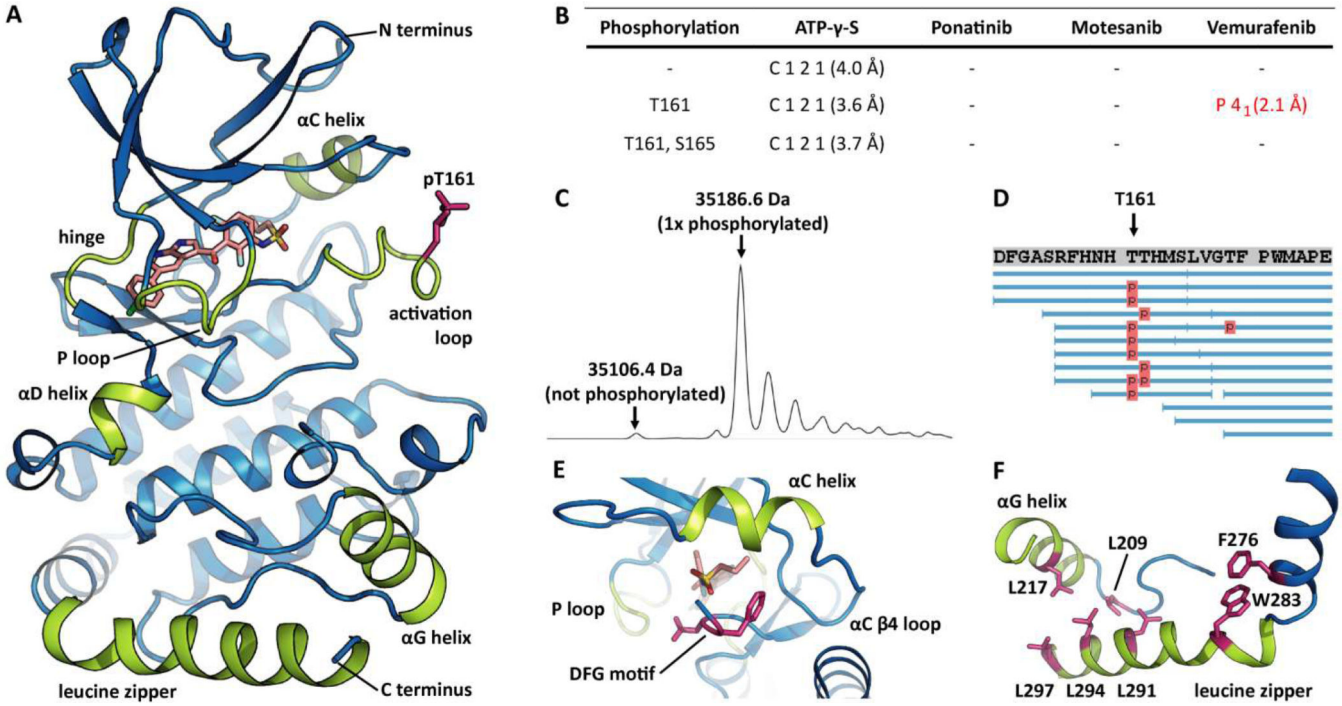

Figure 2.

(A) Crystal structure of $ZAK_{5–309}$ in complex with vemurafenib. Kinase structural elements are highlighted in green. Phosphorylated T161 is shown in red. **(B)** Attempts crystallizing differentially phosphorylated ZAK variants with diverse inhibitors. Listed are the space groups and the diffractions of the obtained crystals. Only the combination of ZAK phosphorylated in T161 and vemurafenib resulted in co-crystals with suitable diffraction properties. **(C)** Intact protein MS spectrum of the monophosphorylated $ZAK_{5–309}$ used for crystallisation. **(D)** Phosphomapping of monophosphorylated $ZAK_{5–309}$. MS/MS spectra have been analysed with PEAKS. The predominant phosphorylation site is T161 within the ZAK activation loop. **(E)** Vemurafenib binds to ZAK in the DFG-in conformation. D151 and F152 are shown in red. **(F)** The N terminal part of the ZAK leucine zipper is tightly attached to the αG helix. Leucine residues forming a hydrophobic surface patch, F267 and W283 are shown in red.

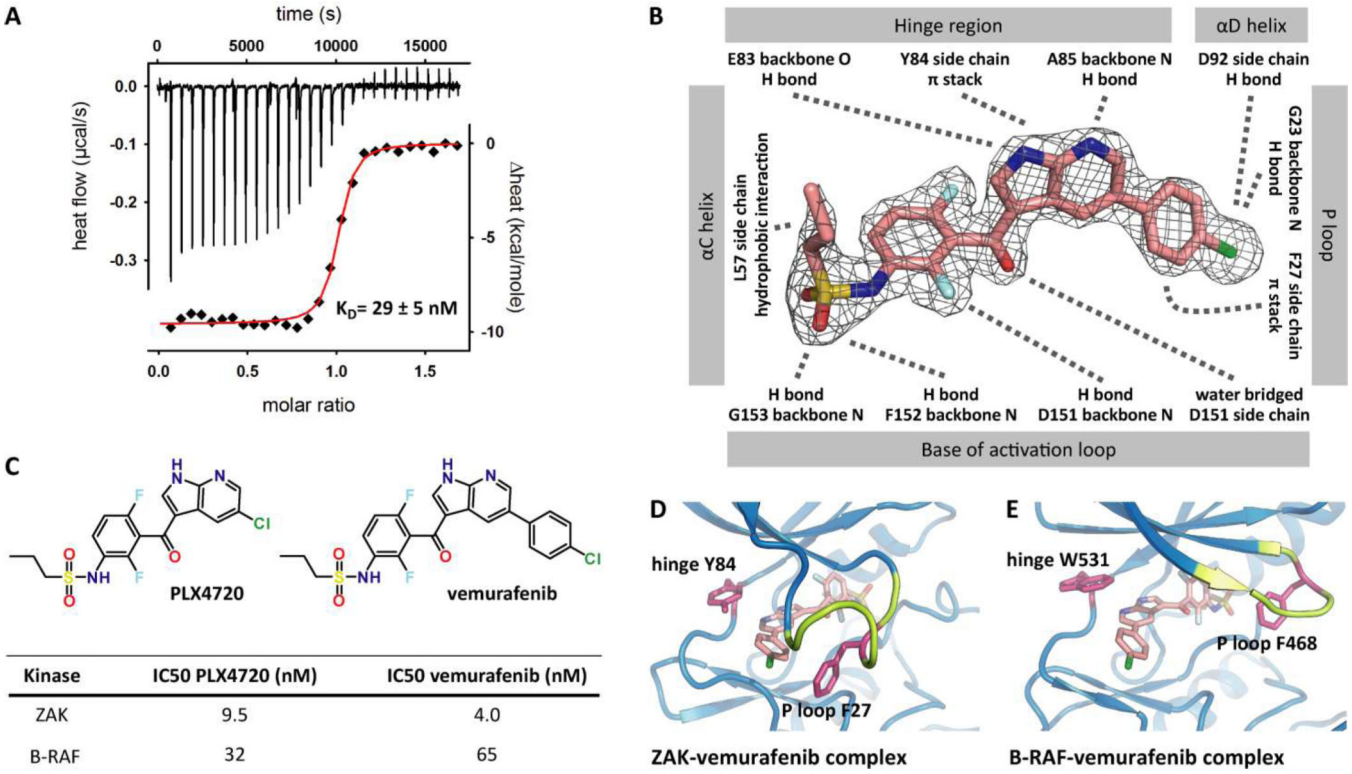

Kinase	IC50 PLX4720 (nM)	IC50 vemurafenib (nM)
ZAK	9.5	4.0
B-RAF	32	65

Figure 3.

(A) Thermodynamic properties of vemurafenib binding to ZAK assessed by ITC. **(B)** Vemurafenib bound to ZAK interacts with a range of kinase structural motifs. The 2mFo-DFc electron density map is contoured at 2.5σ. **(C)** IC50s of PLX4720 and vemurafenib for ZAK and B-RAF as determined by Vin *et al.*[21] **(D)** Vemurafenib binding to ZAK induced a kinked P loop conformation. F27 formed a π stacking interaction with the vemurafenib chlorophenyl ring. **(E)** Vemurafenib binding to B-RAF stabilized an extended P loop conformation. F468 did not interact with vemurafenib (PDB ID 3OG7).